Nucleation and Growth of Single-Walled Carbon Nanotubes: A Molecular Dynamics Study

Feng Ding,* Kim Bolton, and Arne Rosén

Experimental Physics, School of Physics and Engineering Physics, Göteborg University and Chalmers University of Technology, SE-412 96, Göteborg, Sweden

Received: July 28, 2004

Molecular dynamics simulations based on an empirical potential energy surface were used to study iron catalyzed nucleation and growth of single-walled carbon nanotubes (SWNTs). The simulations show that SWNTs grow from iron-carbide particles at temperatures between 800 and 1400 K, whereas graphene sheets encapsulate the particle at temperatures below 600 K and a three-dimensional soot-like structure is formed above 1600 K. Nucleation of these carbon (C) structures can be divided into three stages: (i) at short times the FeC particle is not saturated in C and all C atoms are dissolved in the particle; (ii) at intermediate times the FeC cluster is highly supersaturated in C and carbon strings, polygons and small graphitic islands nucleate on the cluster surface; (iii) at longer times the FeC cluster is supersaturated in C and, depending on the temperature, the graphene sheet, SWNT, or soot-like structure is grown. At low temperatures the kinetic energy is not sufficient to overcome the attractive forces between the particle and the graphitic islands (that are formed in stage ii) and, because these islands cannot lift off the particle, a complete graphene sheet grows around the cluster. At temperatures above 800 K the kinetic energy is sufficiently high to overcome these attractive forces so that the graphitic island lifts off the particle to form a cap. Between 800 and 1400 K theses caps grow into SWNTs, and at temperatures larger than 1600 K the large number of defects in the growing carbon structure produces a soot-like structure. The calculations also reveal that the growing SWNT maintains an open end on the cluster due to the strong bonding between the open nanotube end atoms and the cluster. The number of defects in the SWNT structure can be reduced by lowering the rate of carbon addition to the FeC cluster.

Introduction

The discovery of multiwalled carbon nanotubes by Iijima in 1991[1] and single-walled carbon nanotubes (SWNTs) by Iijima[2] and Bethune[3] in 1993 initiated rapid and extensive progress in the field of carbon nanotechnology. This includes the production of aligned single-walled carbon nanotubes that are several millimeters long,[4] identification of methods that yield large quantities of high quality SWNTs[5] and ropes of SWNTs that have a narrow diameter distribution.[6] The exceptional physical and chemical properties of SWNTs makes them interesting candidates for a vast number of applications.[7] Depending on their chirality, SWNTs may be semiconducting or metallic and can thus be used as transistors and interconnects in electronic circuitry.[8] However, methods to produce SWNTs that have a desired chirality have still not been identified. One can speculate, for example, on the possibility of achieving this goal by extending preexisting nanotubes (that have a desired chirality) or to control the nanotube chirality by selecting certain catalyst or growth conditions. An increased understanding of the SWNT growth mechanism will enable us to address these issues.

The three most common methods of producing SWNTs are arc discharge,[2,3] laser ablation[9] and catalyst chemical vapor deposition (CCVD).[10−12] SWNTs are usually produced in the presence of transition metal particles (e.g., Fe, Co, Ni or their alloys). In arc discharge and laser ablation methods these metal atoms or clusters "float" in the vapor (i.e., they are not on a substrate), whereas in CCVD methods they may float in the vapor[11] or be on a substrate.[12] Substrate effects are important for SWNT growth when the catalyst particle is initially on a substrate,[13] but they are not present in the floating catalyst methods. In these methods the catalyst particles form from vapor phase atoms, molecules and clusters, and their size may increase during SWNT growth. Also, it is often observed that one end of the SWNT is closed whereas the opposite end is embedded in the catalyst particle, which has a diameter similar to that of the SWNT.[14]

Although there has been large progress in the experimental production of SWNTs, the growth mechanism is still poorly understood. In situ studies of SWNT growth, which yield detailed information about the initial stages of the growth process, have only recently appeared.[15] Many issues, such as the mechanism by which the catalyst particle maintains an open nanotube end and heals defects, the key aspects that determine the SWNT chirality, and the detailed mechanism of SWNT nucleation on the catalyst particle, are not well understood. This lack of detailed understanding hinders the continued improvement in experimental production methods.

In CCVD methods the carbon (C) atoms that form the SWNT are introduced as a feedstock such as CO, ethane or other carbon-rich gases.[11] It is generally believed that, for these methods, the metal cluster has two important and distinct roles in the growth process. The first is to act as a catalyst and break the bonds of the carbon feedstock molecules to produce C atoms.[8] The second is to act as a solvent for the C atoms before and during SWNT growth. The vapor−liquid−solid (VLS) model is often invoked to describe the second stage.[16−18] According to the VLS model, carbon and metal atoms that are initially in the vapor phase form a liquid metal−carbide particle,

* Corresponding author. E-mail: fengding@fy.chalmers.se.

10.1021/jp046645t CCC: $27.50
Published on Web 10/14/2004

and when this particle is supersaturated in carbon, solid-phase SWNTs are grown. Although the VLS model does not require a detailed description of the SWNT growth mechanism, it may be expected (and is shown below) that growth is nucleated by small graphitic islands that form on the supersaturated cluster surface. For example, it has been speculated that the islands grow in size as more carbon atoms precipitate on the surface, and when the island covers half of the catalyst particle, it lifts off the particle surface and forms the SWNT.[18] Because the island covers half of the particle before lifting off the surface, the SWNT has the same diameter as the particle. Although the VLS model is easy to understand and is in good agreement with experiment, it does not provide a detailed, atomic-level description of the nucleation and growth process. For example, it is not evident why only one graphitic island forms at the initial stage of nanotube growth or why the island needs to cover half of the catalyst particle before it can lift off the surface. In addition, the model does not explain the experimental observation that SWNTs can only grow within a certain temperature interval.[19]

Theoretical calculations indicate that the open ends of single- and double-walled carbon nanotubes tend to close in the absence of catalyst atoms.[20,21] This results from the pentagonal defects that are formed when carbon atoms add at the open end. It is therefore often believed that catalytic repair of these defects is crucial for maintaining the open ends of growing SWNTs. Also, density functional theory (DFT) calculations show that one or more catalyst atoms that are adsorbed on the open end of a SWNT may be able to fix these types of defects. This forms the basis of the scooter mechanism,[22] where one or few catalyst atoms that are absorbed on the open end of the SWNT rapidly diffuse (scoot) along the open nanotube end and heal defects. In this way hexagons are formed from the defects and the nanotube end does not close. However, first-principles MD simulations indicate that a single catalyst atom on the open SWNT end cannot heal all of the pentagonal defects that are formed at 1500 K, and tube closure is thus inevitable.[23] It appears, therefore, that a catalyst particle with more than one atom, such as found in experiments, is required to maintain the open end that is important for SWNT growth.

Direct dynamics simulations based on DFT theory have also been used to study SWNT nucleation and growth.[17] The time development of the electron density, which is expected to play a critical role in catalytic reactions, is explicitly included in these methods. Unfortunately, the computational cost of this method severely limits the size of the system that is simulated as well as the simulation time (several tens of picoseconds, which is not sufficient to allow for SWNT nucleation, have been simulated). Recently, molecular dynamics (MD) simulations based on an empirical potential energy surface (PES) were used to simulate SWNT nucleation under laser ablation and CCVD conditions.[24] Trajectories that were sufficiently long to allow for nucleation of graphitic cap-like and SWNT structures were propagated, but temperatures (2000−2500 K) that are far higher than those used in CCVD experiments were required.

Several important aspects for growing well-structured SWNTs, as identified by previous experimental and theoretical studies, can be summarized as follows:

(1) A suitable catalyst particle is essential for producing high quality SWNTs.

(a) Because a single catalyst atom does not appear to be sufficient to maintain an open end of the growing SWNT, the catalyst particle must be bigger than some critical size. It is expected that this size is similar to the diameter of the thinnest free-standing SWNTs that can be obtained experimentally: 0.6−0.7 nm.[25]

(b) In CCVD experiments the catalyst is usually required to decompose the feedstock to release carbon atoms (although a small amount of gaseous carbon atoms can adsorb on the growing SWNT in some cases).

(c) The catalyst particle must act as a solvent for the carbon atoms (required by the VLS model).

(d) The particle must maintain an open end of the growing nanotube (so that long nanotubes can be grown).

(e) If defects cannot be thermally annealed under the experimental condition, then the catalyst particle must heal these defects when they form at the growing end of the SWNT (so that pristine nanotubes can be grown).

(2) A suitable temperature is required (e.g., the lowest temperature where SWNTs are grown and that is reported by S. Maruyama et al. is 823 K[26] and, as far as we are aware, the highest reported temperature for CCVD grown SWNTs is 1473 K.[27] This upper temperature limit is also very similar to the highest oven temperature used in laser ablation methods[28]).

(3) A suitable feedstock and feedstock pressure is required.

In this contribution we report results of an MD study of SWNT nucleation and growth on an FeC particle. In contrast to previous studies,[17,24] these simulations are based on an analytic PES that yields the correct FeC phase behavior,[40] which is important in the VLS model, and the decrease in FeC cluster melting point with decreasing cluster size.[40] Also, for the first time, simulated SWNT nucleation occurs between 800 and 1400 K, which is similar to the temperature interval for CCVD SWNT production. As discussed below, the simulations reveal the role of the metal particle and the details of the SWNT growth process, such as the initial cap formation, the mechanism of maintaining an open end of the growing nanotube, and the inclusion and healing of defects in the nanotube structure at different growth temperatures and carbon concentrations. Based on these results, a detailed VLS SWNT growth model is presented.

Potential Energy Surface and Simulation Details

A simple illustration of the components of the PES is shown in Figure 1. It is well-known that the interaction between carbon atoms that are dissolved in FeC particles is very weak compared to carbon atoms that form part of a graphene structure, and that they do not tend to aggregate before the FeC particle is supersaturated.[29] Hence, dissolved C atoms are not covalently bonded to each other, as they are when they precipitate on the surface and form graphitic structures. On this basis, the carbon atoms are separated into two classes in our PES description, i.e, the dissolved (C_D) and precipitated (C_P) carbon atoms. The criterion that distinguishes between these two types of atoms is that the atom has precipitated (C_P) if the number of neighboring Fe atoms (where the Fe−C distance is smaller than 2.3 Å) is less than 5. This number is used in the simulation because most carbon atoms inside the Fe−C cluster have 7−8 neighboring iron atoms. Changing this value to 4 or 6 neighboring atoms does not affect the results presented here.

The interaction between C_D atoms is described by a Lennard-Jones (12−6) potential: $E = 4\epsilon[(\sigma/r)^{12} - (\sigma/r)^6]$ with $\epsilon = 0.4396$ kJ/mol and $\sigma = 3.851$ Å.[30] This interaction, where the repulsion is the dominant effect and the well-depth is very small, acts merely to prevent aggregation of dissolved atoms. The Brenner potential,[31] which has successfully been used in many previous studies to simulate carbon nanotube dynamics,[24] is used

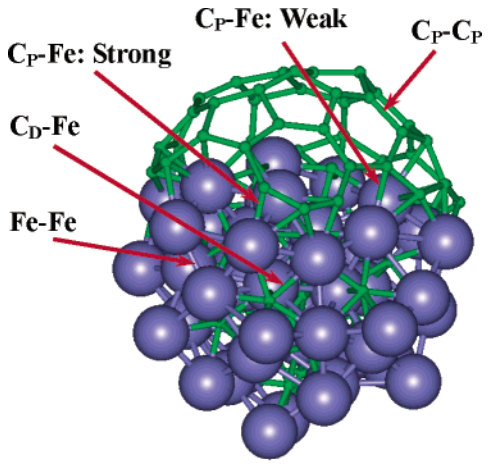

Figure 1. Potential energy surface (PES) used for the simulation: Fe−Fe, the many body potential between iron atoms; C_D−Fe, Johnson potential; C_P−Fe:Strong, the strong interaction between the precipitated bond-unsaturated carbon atoms and the iron atoms; C_P−Fe:Weak, the weak interaction between the precipitated bond-saturated carbon atoms and the iron atoms; C_P−C_P, Brenner potential. The C_D−C_D and C_D−C_P interactions are not shown in the figure.

to describe the interaction between the C_P atoms. The interaction between C_D and C_P atoms is described by the same Lennard-Jones (12−6) potential given above and, similarly to the C_D-C_D interactions, this merely to prevents the distance between the C_D and C_P carbon atoms from becoming too short. It can be noted that moderate (20%) changes in the L−J parameters does not affect the simulation results presented here.

The Johnson potential provides a valid description for carbon in α-Fe, martensite and cementite, and has been used to simulate C dissolved in liquid Fe.[32−35] The interaction between iron and dissolved carbon atoms is

$$E_{\mathrm{Fe-C_D}} = \sum_{i<j} -\epsilon\left[2\left(\frac{\frac{r_C}{r_0}-\frac{r_{ij}}{r_0}}{\frac{r_C}{r_0}-1}\right)^3 - 3\left(\frac{\frac{r_C}{r_0}-\frac{r_{ij}}{r_0}}{\frac{r_C}{r_0}-1}\right)^2\right]H(r_C - r_{ij})$$

where

$$H(r_C - r_{ij}) = \begin{Bmatrix} 0 & r_C - r_{ij} < 0 \\ 1 & r_C - r_{ij} \geq 0 \end{Bmatrix}$$

is a step function that truncates the Fe−C_D interaction energy and r_{ij} is the distance between the ith iron and jth carbon atoms. The constants $\epsilon = 0.35$ eV, $r_0 = 1.94$Å and $r_c = 2.53$Å are obtained by fitting to experimental data for α-Fe (the migration energy for C_D atoms, the activation volume of C_D migration and the vacancy-C_D binding energy).

The interactions between the C_P and Fe atoms is important for the nucleation and growth of SWNTs, as well as the catalytic healing of defects. According to sp^2 hybridization theory, C_P atoms at the center of graphitic islands are bond saturated (each atom is connected to three other atoms and thus has no dangling bonds) and interact with other atoms via weak π bonding. Hence, C_P atoms that form part of the SWNT or precipitated graphitic islands, and that are not end/edge atoms, interact very weakly with Fe atoms. This is in agreement with the ab initio (PW/GGA) adsorption energy of an iron atom on a (6, 6) carbon nanotube surface of only 0.8 eV.[41] On the other hand, the interaction between carbon atoms at the open end of a SWNT (which have at least one dangling bond) and iron clusters is very strong. This is also the case for C atoms at the edge of precipitated graphitic islands, and for precipitated C atoms and dimers. For example, DFT bond energies of a free carbon atom on an Fe_{2-6} cluster are 5.5−7.0 eV.[42] In the PES used here, the interaction between precipitated carbon atoms and iron atoms are represented by the Johnson potential with the well depth parameter (ϵ) fitted to DFT results.[41,42] For bond saturated carbon atoms, $\epsilon = 0.14$ eV, which yields the same absorption energy for an Fe atom on the surface of a (6, 6) carbon nanotube as that obtained from DFT. For bond unsaturated C atoms, $\epsilon =$ 1.5 eV, which yields an adsorption energy of a carbon atom on an Fe cluster surface of 4.5−6.0 eV. Although the present PES includes the effects of these different types of iron−carbon interactions, in reality there may be many more "types" of interactions (e.g., the interaction between a C_P atom at the SWNT end with Fe atoms may also depend on the number of neighboring Fe atoms). Thus, because these effects are included in the PES in a very simple way, some important details may be omitted. However, it is important to note that the results presented in this paper are not sensitive to the Fe−C_P well depth parameters, and simulations indicate that a 20% change in these values does not significantly change the simulated SWNT structures or growth mechanisms reported here.

Many-body interaction potentials that are based on the second moment approximation of the tight binding model[36] are suitable for studying the thermal properties of pure[37] and alloy[38] transition metal systems. The interaction energy between iron atoms can be written as a sum of Born−Mayer type repulsive and many-body attractive energy terms,

$$E_{\mathrm{Fe-Fe}} = \sum_{i\neq j} A\exp\left[-p\left(\frac{r_{ij}}{r_0}-1\right)\right] - \left\{\sum_{i\neq j}\xi^2\exp\left[-2q\left(\frac{r_{ij}}{r_0}-1\right)\right]\right\}^{1/2}$$

where r_{ij} is the distance between the ith and jth iron atoms. The constants $A = 0.13$ eV, $\xi = 1.62$ eV, $p = 10.50$, $q = 2.60$, and $r_0 = 2.553$ Å are obtained by fitting the cohesive energy, lattice parameter and elastic constants of the γ Fe (fcc structure).[39]

The PES described above has been used to study the thermal properties of FeC cluster systems. MD simulations based on this PES yielded the correct trends of the FeC phase diagram, where a eutectic was found at 20% carbon content by atom number. In addition, the correct $N^{-1/3}$ dependence of the cluster melting point on the number of atoms, N, in the cluster was obtained.[40] These results support the validity of using this PES to study the thermal dynamics of FeC systems, and yields correct trends (phase behavior and melting point dependence on cluster size) that are important in the VLS description of SWNT growth.

The simulations presented here mimic CCVD growth of SWNTs using floating catalyst particles. For these experimental methods the temperature is constant and fairly well controlled and, as discussed above, there are no substrate effects. However, it is important to note that this study also addresses issues that are relevant to other experimental growth techniques (e.g., arc discharge, laser ablation, and CCVD on a substrate). These issues, which do not depend on fixed temperature or the presence of a substrate, include the mechanism for the formation of the initial graphite cap, the role of the catalyst particle in maintaining an open end on the growing SWNT, and the mechanism by which SWNT defects are healed.

Trajectories are initialized by annealing the pure iron cluster, Fe_N, to its minimum energy structure and then heating it to the desired temperature. The cluster is then propagated at this

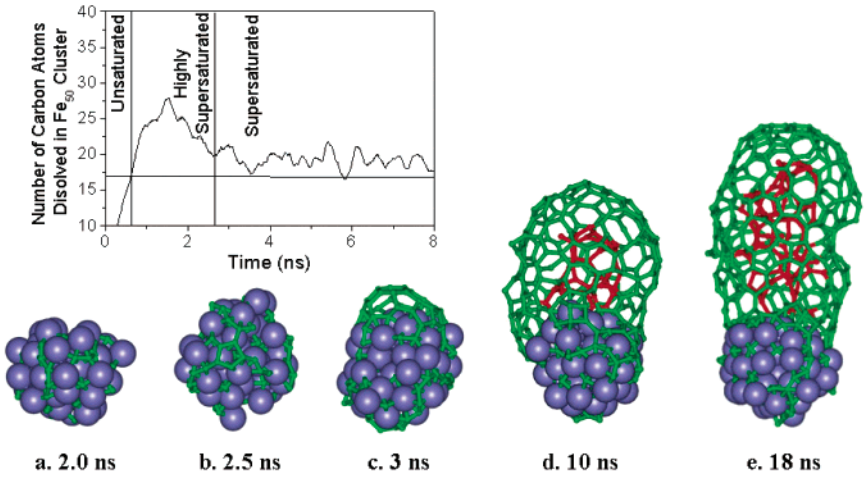

Figure 2. Snapshots during SWNT growth at 900 K. The cluster contains fifty Fe atoms, and one carbon atom is added to the central part of the cluster every 40 ps. Iron atoms are represented as balls and carbon atoms as a stick-like structure. Carbon atoms inside the tubular structure are shown in red. The time dependence of the dissolved carbon content is shown in the inset.

temperature for 100 ps to ensure thermal equilibrium, after which carbon atoms are inserted into the central part of the cluster. The rate of carbon atom insertion varies from 1 atom per picosecond to 1 atom per several hundreds of picoseconds and is typically 1 atom per 40 ps. This carbon insertion rate which, as discussed below, determines the growth rate, is more than 4 orders of magnitude larger than the experimental upper limit[4,43] but is required for simulation of SWNT growth within a reasonable computational time. The Berendsen velocity scaling method[44] was used to maintain the cluster at the desired temperature, the simulation time step was 1 fs, and about 24 CPU hours was needed to propagate a typical 10 ns trajectory on an AMD 900 MHz PC.

In CCVD experiments the C atoms that form the SWNT are obtained from feedstock decomposition at the surface of the cluster. It should thus be noted that simulations where C atoms were added at the surface of the cluster gave results similar to those presented here. In fact, for sufficiently slow rates of C addition (e.g., lower than 1 atom per 10 ps at 900 K), no differences in the growth mechanism were observed. This is expected because C atoms can diffuse into the Fe cluster before the SWNT nucleates under these conditions. It may also be noted that we do not consider C atoms that diffuse to the cluster via the substrate (because only floating FeC clusters are studied) or along the SWNT wall (because only minor quantities of gaseous C is expected under thermal CCVD conditions). In addition, under all conditions (temperature, cluster size and C atom addition rate) studied here the C dissolves rapidly into the cluster and surface diffusion does not dominate. Hence the results may not be relevant to larger Fe clusters that may be in the solid state during carbon nanotube growth, and where surface diffusion may dominate.

Results and Discussion

Nucleation of Single-Walled Carbon Nanotubes. Figure 2 shows snapshots during the nucleation of a SWNT at 900 K on an Fe_{50} cluster. The SWNT growth mechanisms on other clusters ($20 \leq N \leq 150$) are similar to that presented here. This work focuses on Fe_{50}, which has a diameter $\approx$1 nm, similar to diameters of the clusters used in some CCVD experiments. Similar structures to those shown in Figure 2 are obtained at all temperatures between 800 and 1400 K, which is the same interval where SWNTs grow in CCVD experiments.[19]

The inset to Figure 2 shows the time dependence of the number of C atoms that are dissolved in the FeC cluster during SWNT growth. The maximum in dissolved carbon content, which is between 0.7 and 2.6 ns, separates the growth process into three distinct stages. In the first stage, from 0 to 0.7 ns, the FeC cluster is not saturated in carbon, so that all carbon atoms are dissolved. The number of (dissolved) carbon atoms increases linearly with a rate that equals the rate of C atom insertion into the cluster (1 atom per 40 ps).

The second stage (from 0.7 to 2.6 ns) is the key stage in SWNT nucleation. At 0.7 ns the FeC cluster is supersaturated in carbon (the term "supersaturated" is used instead of "saturated" for the sake of consistency with previous work[45]). Despite this, the dissolved carbon concentration continues to increase until the FeC cluster reaches a highly supersaturated state at about 1.5 ns. Although a few carbon atoms precipitate on the cluster surface between 0.7 and 1.5 ns, they are randomly distributed on the surface and can dissolve back into the cluster. From 1.5 ns, when the number of dissolved C atoms is at a maximum, there are a larger number of precipitated carbon atoms, and these nucleate the formation of small carbon clusters such as strings and small polygons. After nucleation of these small clusters there is a decrease in dissolved C content because more carbon atoms precipitate on the surface and the strings and polygons grow into graphitic islands. After 2.6 ns the dissolved carbon concentration is constant and large graphitic islands are formed by the growth or coalescence of smaller islands.

At the beginning of the third stage, which starts at 2.6 ns, the graphitic islands are sufficiently large to allow them to lift off the cluster surface. Analysis of the trajectories show that this critical island size (needed to lift off the cluster) is about 0.6 nm; i.e., the island contains about 15−20 carbon atoms or 5−7 polygons. When the graphitic island lifts off the surface, it forms a graphitic cap that increases in diameter and length as more dissolved carbon atoms precipitate and bond at the open cap edge. The cap diameter increases until it is the same as the diameter of the cluster. At this stage a SWNT that has a similar diameter to that of the FeC cluster has been formed, and it grows in length as more carbon atoms are incorporated at its open end.

Cap Formation. The simulations identify three possible routes by which graphitic islands grow into caps on the cluster surface. More than one carbon island typically forms on the cluster surface during the second stage of SWNT nucleation. The number of islands depends on the FeC cluster size, with more islands being formed on larger clusters. For the $Fe_{50}C$

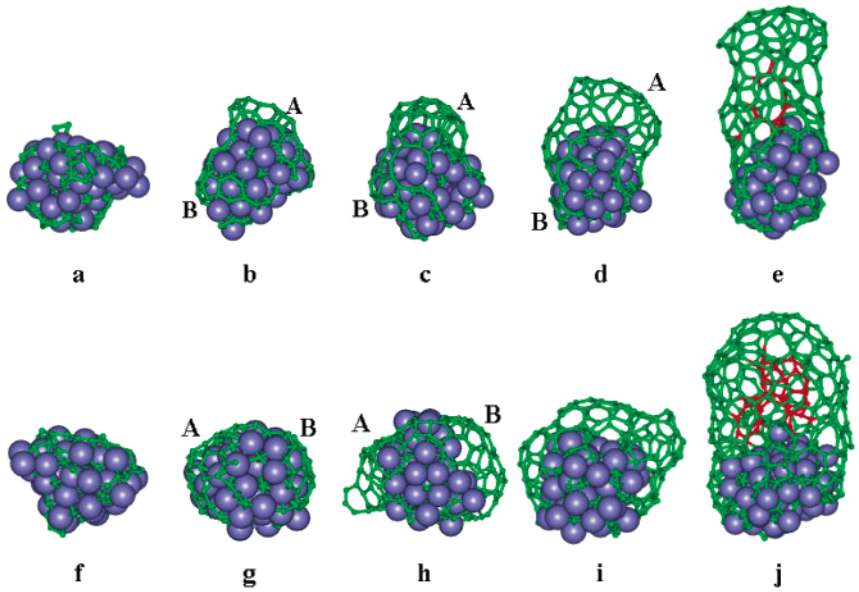

Figure 3. Two of the three cap formation mechanisms that were identified from the $Fe_{50}C$ simulations (Figure 2 illustrates the third mechanism). Panels a−e show that even though two large islands, A and B, are present, only the larger one, A, grows into the cap whereas the smaller one, B, dissolves back into the cluster. Panels f−j illustrate the mechanism where two large islands, A and B, lift off the surface to form caps, which subsequently coalescence into a single large graphitic cap. The simulation conditions and color coding are the same as those in Figure 2.

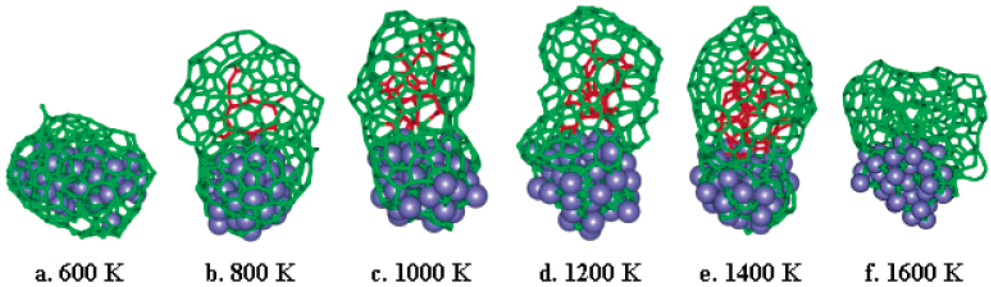

Figure 4. Graphene (a), SWNT (b−e) and soot (f) structures obtained between 600 and 1600 K. The simulation conditions and color coding are the same as in Figure 2.

cluster discussed here, 2−4 islands are typically formed. Larger islands typically grow faster than smaller ones, and the smaller islands can also dissolve back into the FeC cluster. In addition, two or more small islands can coalescence to form a larger island. Both the dissolving and coalescence processes reduce the total number of islands, and the number of large islands that exist at the end of the second stage is less than the number of smaller islands that are initially nucleated. For the $Fe_{50}C$ cluster, 1 or 2 large islands are typically found at the end of the second stage. If there is only one large carbon island, it lifts off the surface to form the graphitic cap that eventually grows into the SWNT (Figure 2 is an example of such case). If there are two large islands, then there are two possible growth scenarios. The first is that only one of the islands (often the larger one) lifts off the surface to form the cap whereas the other island dissolves back to the FeC cluster (see Figure 3a−e). The second scenario is that both of the islands lift off the surface to form two graphitic caps. However, for the $Fe_{50}C$ cluster discussed here, these caps do not each form their own SWNT, but they coalesce into one graphitic cap that grows into a single SWNT (see Figure 3f−j). None of the trajectories (more than 100 that have been propagated) indicated that two or more SWNTs can grow on the $Fe_{50}C$ surface (diameter $\approx$ 1 nm). This is in accordance with the experimental observation that single isolated SWNTs grow from small catalyst particles.[46]

The mechanism of graphitic island nucleation and cap formation is very similar to the nucleation mechanism of small liquid drops in supersaturated vapor.[47] First, highly supersaturated conditions are needed to initiate nucleation. Second, small islands/drops are less stable than larger ones. Also, the reduction in dissolved carbon concentration that occurs when the islands grow in size (during the second stage) prevents the nucleation of more small islands on the cluster surface.

Temperature Dependence of the SWNT Structure: Inducing and Healing Defects. As discussed above, SWNTs grow at all temperatures between 800 and 1400 K. As shown in Figures 2 (for 900 K) and 4b−e (for 800, 1000, 1200, and 1400 K, respectively), all SWNTs contain defects. A histogram showing the number of polygons that are found on the surface of SWNT structure (i.e., considering only the green atoms in these figures) over this temperature range is shown in Figure 5. It is clear that, for all the temperatures, there are more hexagons than the other polygons. However, there are far more defects (nonhexagonal polygons) than what is found in a perfect SWNT (Euler's theorem for polyhedra[48] states that only six pentagons are needed in the cap of each SWNT). It is also evident that, in addition to the pentagons and heptagons, some quadrangles and octagons are present. This large number of defects indicates that carbon atoms do not append to the open end of the growing SWNT in such a way that only hexagons are formed. That is, the local minima on the PES for the nonhexagonal structures are sufficiently stable on the simulation time scale to induce formation of these structures.[31] Also, the number and distribution of the different defects is the same for all temperatures between 800 and 1400 K. This shows that the defects are not thermally healed at these relatively low tem-

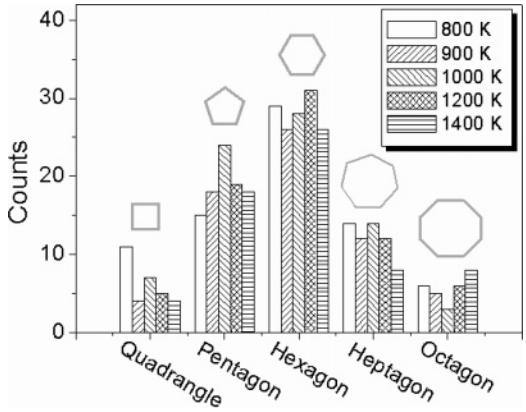

Figure 5. Distribution of polygons in the simulated SWNT structures at different temperatures.

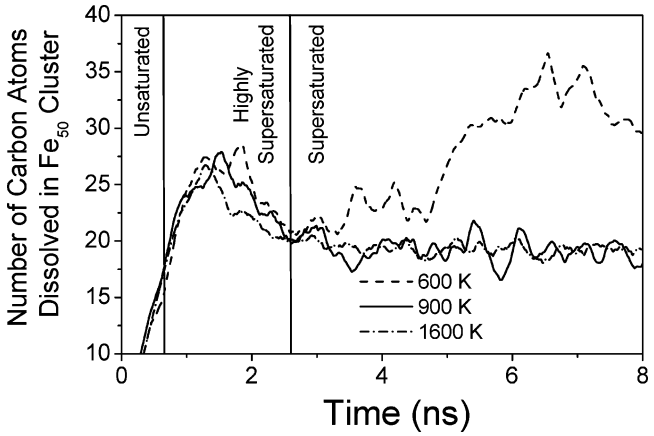

Figure 6. Dissolved carbon content in the $Fe_{50}C$ cluster during the growth of a graphene sheet at 600 K (dashed line), a SWNT at 900 K (solid line), and the soot-like structure at 1600 K (dot−dashed line).

peratures (800−1400 K compared to the melting point of 4100 K for graphite) during the relatively short simulation time (about 10−20 ns compared to the experimental growth time of several seconds or longer). Hence, the thermal annealing of defects that may be effective under experimental growth conditions is not observed in the simulations. A second reason for the large number of defects formed in the simulated growth is that some carbon atoms precipitate and attach to the inside of the cylindrical SWNT structure. These atoms, which are shown in red in Figures 2−4, create many defects, especially quadrangles and octagons. Other reasons for the large number of defects in the simulated SWNT structures, such as the high rate of C addition to the FeC cluster, are discussed below.

Encapsulation of the FeC Cluster at 600 K and Growth of a Soot-Like Structure at 1600 K. Encapsulation of the FeC clusters by a graphene layer and the growth of a soot-like structure at 600 and 1600 K, respectively, are shown in Figure 4. The number of carbon atoms that are dissolved in the FeC cluster during the growth of these structures is shown in Figure 6 (the corresponding data for SWNT growth at 900 K, which is shown in Figure 2, are included for comparison). A similar maximum in the dissolved carbon content between 0.7 and 2.6 ns that is found during SWNT growth is also found during the growth of the graphene and soot-like structures. In fact, the first (0−0.7 ns) and second (0.7−2.6 ns) stages of the growth process are very similar to those discussed for SWNT growth, where precipitated carbon atoms nucleate strings and polygons that form larger graphitic islands at the end of the second stage. The difference in the growth processes arises in the third stage. At low temperatures (600 K and below) the available kinetic energy is not sufficient to overcome the attraction between the graphitic island and the FeC cluster surface, and the island does not lift off the surface but continues to grow until it encapsulates the cluster (Figure 4a). At high temperatures (1600 K and above), the graphitic cap lifts off the cluster surface but the number defects that are formed is so large that a 3D soot-like structure is formed instead of a SWNT. That is, the large kinetic energy at these temperatures allows many of the local minima on the PES, which are associated with defects, to be sampled and the soot-like structure is grown. In fact, Figure 4b−e shows that an increase in temperature leads to more carbon atoms attaching to the inside of the SWNT (shown in red) and hence more defects are formed with increasing temperature. At 1600 K the number of these defects is so large that the cylindrical SWNT structure is destroyed and the soot-like structure is produced.

In agreement with the simulated growth mechanism discussed above, recent studies[49,50] indicate that the kinetic energy (or temperature) plays an important role in determining whether the graphitic islands can lift off the cluster surface. At 800 K and above the kinetic energy is sufficiently large to overcome the adhesive energy between the cluster surface and the graphitic island, and graphite caps that grow into SWNTs or soot-like structures are produced. At 600 K and below the adhesive energy dominates over the kinetic energy, and the graphitic island does not lift off the cluster surface but grows in size until the FeC particle is encapsulated. When this occurs in CCVD experiments the catalyst particle is poisoned because the feedstock molecules cannot come into contact with the metal surface to produce carbon atoms. The number of dissolved carbon atoms in the metal cluster is thus constant, or decreases if additional graphene layers are formed. In contrast, carbon atoms are added to the central part of the cluster in the simulations and, because carbon atoms cannot easily precipitate once the cluster is covered by a graphene layer, the number of dissolved carbon atoms increases once the cluster is encapsulated (the dashed line in Figure 6 increases during stage three). This increase is thus an artifact of the simulation procedure. It should also be noted that, because decomposition of the feedstock is not explicitly included in the simulation, a possible change—or even cessation—of catalytic decomposition rate due to increasing C content of the cluster is not included in the simulation. Hence possible "poisoning" of the cluster due to increasing C content is not considered.

At 1600 K and above soot-like structures are grown, even though the large graphitic islands that lift off the cluster have similar structures to those formed at intermediate temperatures. The lowest temperature (1600 K) that is required for the simulated growth of soot-like structures is very similar to highest temperature where SWNTs are grown in CCVD experiments. As far as the authors are aware, no CCVD experiments report production of SWNTs at temperatures higher than 1600 K, although many report growth of SWNTs at 1473 K (1200 °C).[27] In addition, the CCVD growth of SWNT at 1200 °C has been reported for all catalyst metals (e.g., Fe,[51] Co,[52] Ni[53]) and different carbon precursors (e.g., benzene,[52] CO,[53] C_2H_2[51]). This suggests that the highest temperature for SWNT growth does not depend on the catalytic metal, which supports the assertion that the SWNT → soot-like transition at 1400−1600 K is determined by the intrinsic properties of the carbon−carbon bonds and not the catalytic properties of the metal cluster.

To validate this assertion and study the mechanism for the soot-like growth at high temperatures, several trajectories based on unrealistic PESs were propagated. The three new PESs were identical to that described before except that the C_P-C_P interac-

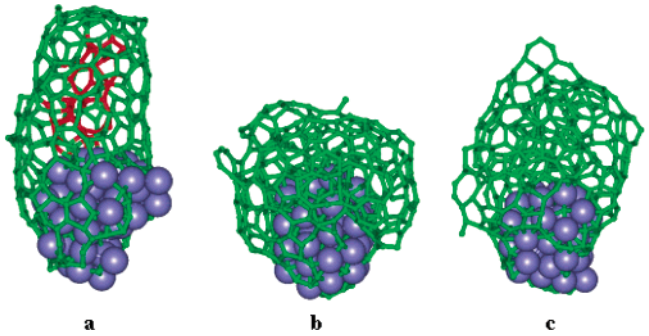

Figure 7. Effect of PES parameters on SWNT and soot growth at 1600 K. A SWNT structure is grown when the C_p-C_p interaction strength is doubled (a), whereas doubling the Fe−Fe (b) or Fe−C (c) interaction strengths does not significantly affect the 3D soot-like structure (compared to Figure 4f). The color coding is the same as that in Figure 2.

tion strength was doubled in the first PES, and the $Fe-C_P$ or Fe−Fe interaction strengths were doubled in the second and third PESs, respectively. The simulation temperature was 1600 K and, similar to the trajectories discussed above, one carbon atom is added to the FeC cluster every 40 ps. The results, presented in Figure 7, show that doubling the C_P-C_P bond strengths led to the growth of a SWNT structure (panel a) instead of the 3D soot-like structure shown in Figure 4f. Moreover, doubling the $Fe-C_P$ or Fe−Fe bond strengths does not significantly affect the soot-like structure. This shows that it is the intrinsic properties of the C_P-C_P bonds that are responsible for the growth of a 3D soot-like structure at high temperatures. According to sp^2 hybridization theory, the three σ bonds of each carbon atom lie in the same plane, and formation of out-of-plane C−C bonds requires more energy. Hence, bonds between carbon atoms in the nanotube wall with those on the inside of the tube structure (red atoms in Figures 2−4) have higher energy than C−C bonds in the SWNT wall, and are only formed when the kinetic energy is sufficiently large. An increase in the number of out-of-plane bonds at high kinetic energies (high temperatures) destroys the tubular structure and the soot-like structure is grown. When the C_P-C_P bond energy is artificially doubled (Figure 7a), the kinetic energy at 1600 K is not sufficient to induce these out-of-plane C−C bonds and a SWNT is grown.

Effect of the Rate of Carbon Insertion into the Cluster Particle on the SWNT Structure. In CCVD experiments the rate at which carbon atoms dissolve into the metal cluster is proportional to the pressure of the carbon feedstock, which is known to play an important role in determining the quality and yield of SWNTs.[27] In the simulations the carbon atoms are inserted about 10 000 times more rapidly into the cluster than in CCVD experiments. Although this difference in carbon dissolution rates (or feedstock pressures) will lead to quantitative differences in SWNT growth rates and structures, the same qualitative effects that are seen experimentally are expected to be observed in the simulations.

Figure 8 shows four typical structures when carbon atoms are inserted into an 800 K FeC cluster at different rates. When the insertion is rapid, the FeC cluster is encapsulated in a graphene layer (e.g., one C atom is inserted every 2 ps in Figure 8a). When the insertion rate is decreased, the graphitic cap lifts off the catalyst surface and a SWNT with many defects is formed (e.g., one C atom is inserted every 5 ps in Figure 8b). Decreasing the insertion rate further leads to fewer defects in the SWNT structure (one C atom is inserted every 10 and 40 ps in Figure 8c,d, respectively). The mechanism by which the C atom insertion rate affects the SWNT structure can be understood with reference to the inset in Figure 2, where it is seen that the dissolved carbon concentration is constant during the third stage of SWNT growth. That is, the rate at which C atoms precipitate on the cluster surface and incorporate into the SWNT structure equals the rate of addition to the cluster. Hence, at large insertion/precipitation rates (e.g., Figure 8a) the graphitic cap does not have time to lift off the cluster surface before a complete graphene sheet grows around the cluster particle. Once the particle is encapsulated, the strong C−C sp^2 bonding is not broken and a SWNT cannot be formed. At lower insertion rates (Figure 8b−d) the graphitic island has time to lift off the surface (i.e., the time scale for cap formation is shorter than that for particle encapsulation). In addition, when the insertion/precipitation rate decreases further (from panel b−d), the precipitating C atoms have time to locate the lowest energy structures in the SWNT and higher quality nanotubes are grown. Even slower insertion rates, such as those found under experimental conditions, are expected to yield high quality SWNTs.

Maintaining an Open End of the Growing SWNT and the SWNT Diameter−role of the Metal Cluster. It has previously been suggested that the formation of defects at the open end of the growing SWNT leads to end closure and growth termination, and that healing of the defects is thus critical for SWNT growth.[22,23,54] However, despite the many defects in our simulated SWNTs, the FeC cluster maintains an open end of the growing SWNT (the end of the SWNT is still open after 30 ns when the length of the tube is about 3 nm). In addition, it has been observed experimentally that the diameter of the SWNT is closely correlated with the diameter of the metal particle,[14] and this is also observed in our simulations.

The carbon atoms at the open SWNT end have one or two "free" bonds (i.e., they are not bond-saturated) and are more chemically active than those that form part of the nanotube or the graphitic cap. The interaction between these end atoms and the iron cluster is very high (e.g., the DFT bond energy of a free carbon atom on an Fe_{2-6} iron cluster is about 5.5−7.0 eV[42]). Our simulations show that it is this large bond energy between the end carbon atoms and the iron cluster that maintains the open end of the growing nanotube. In addition, enthalpy can be substantially reduced when the number of bonds between the nanotube end and the cluster is maximized. This is achieved when the diameter of the SWNT is at a maximum, i.e., when it is the same as the diameter of the FeC cluster. Thus, in agreement with experimental observations, the SWNT diameter is similar to that of the FeC cluster. This is also valid for particles that are larger than the Fe_{50} cluster discussed above. For example, Figure 9 shows that for an Fe_{150} cluster, even though the initial graphitic cap has a smaller diameter than the cluster, the cap diameter increases until it is equal to that of the cluster. In this way the number of nanotube end atom−metal bonds is maximized.

Conclusion

The nucleation mechanism of graphene sheets, SWNTs and 3D soot-like structures, that were observed in the MD simulations and are discussed above, are summarized in Figure 10. The following key processes are evident:

a. The growth mechanism can be divided into three successive stages for all carbon structures.

b. During the first stage all carbon atoms are dissolved in the cluster.

c. At the beginning of the second stage, when the cluster is supersaturated in carbon, a few carbons atoms precipitate on the cluster surface. However, these atoms can dissolve back

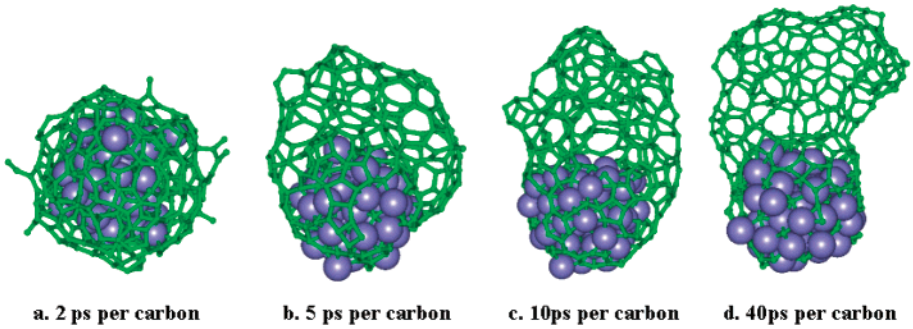

Figure 8. Effect of C insertion rate on the growth process. Inserting one C atom every 2 ps leads to encapsulation of the particle (a) whereas decreasing the insertion rate leads to SWNTs with fewer defects (from b to d). The color coding is the same as that in Figure 2 and the temperature is 800 K.

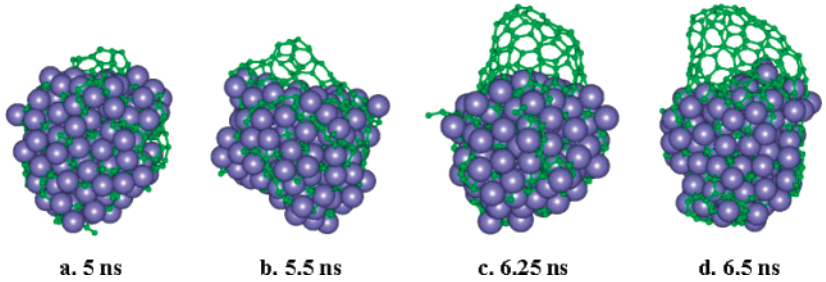

Figure 9. Nucleation of a SWNT from an Fe_{150} cluster. The diameter of the graphitic cap increases during the growth process until it equals the diameter of the cluster. The temperature is 1100 K and the color coding is the same as in Figure 2.

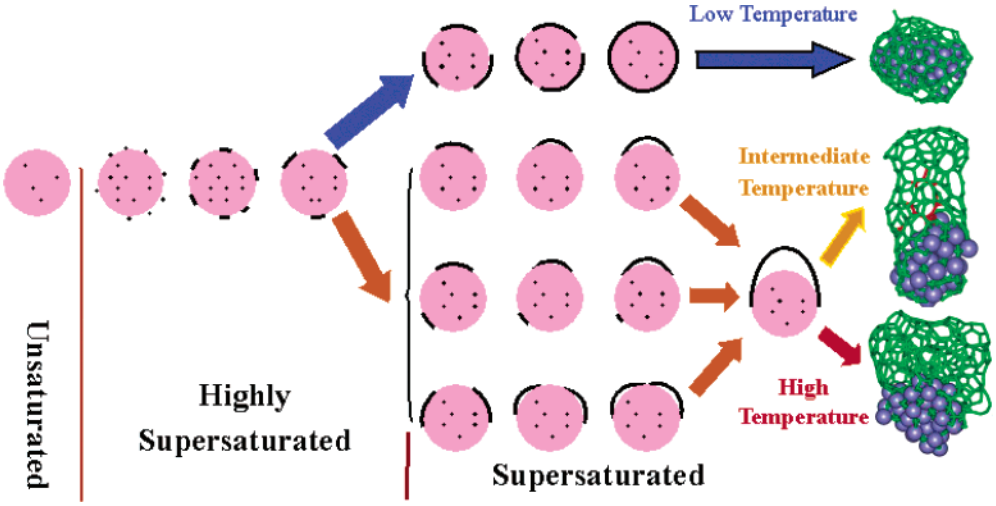

Figure 10. Detailed vapor−liquid−solid model of SWNT growth at different temperatures.

into the cluster and the carbon concentration continues to increase until the cluster is highly supersaturated in carbon.

d. As the dissolved carbon concentration increases during the second stage, an increasing number of carbon atoms precipitate on the cluster surface and form carbon strings and polygons. The dissolved carbon concentration begins to decrease as these strings and polygons nucleate graphitic islands.

e. Some islands dissolve back into the cluster and others grow into larger islands. The dissolved carbon concentration continues to decrease until a supersaturated level is reached, at which stage large graphitic islands have formed.

f. At low temperatures the islands do not lift off the cluster surface and the FeC cluster is encapsulated in a graphene sheet.

g. At intermediate temperatures a number of scenarios are possible: (i) If a single large island is present, it lifts off the cluster surface (when its size is about 0.6−0.7 nm) to form a graphite cap. The diameter of the cap increases until it equals the diameter of the cluster. (ii) If two islands are present, then either the larger one lifts off the cluster to form a cap and the smaller one dissolves back into the FeC cluster or, if two or more islands lift off the surface and form caps, then their diameters increase until they coalescence into a single large cap.

h. When the diameter of the cap is similar to that of the cluster, the precipitating carbon atoms join to the open end of the SWNT and increase the SWNT length.

i. High temperatures lead to an increased number of defects and a 3D soot-like structure is formed.

The simulations also reveal other details of the growth mechanism. For example, it is seen that the growing SWNT maintains an open end on the FeC particle due to the strong bonding between the SWNT end atoms and the particle. Similarly, the SWNT-particle enthalpy is minimized when the SWNT and FeC cluster have similar diameters, and this leads to the growth of SWNTs that have diameters similar to those of the metal clusters, as seen experimentally.

Acknowledgment. We are grateful for the time allocated on the Swedish National Supercomputing facilities and for financial support from the Swedish Research Council, the Swedish Foundation for Strategic Research (CARAMEL consortium), and the Royal Society of Arts and Sciences in Göteborg. We also acknowledge fruitful discussions with Peter Eklund.

References and Notes

(1) Iijima, S. *Nature* **1991**, *354*, 56−58.

(2) Iijima, S.; Ichihashi, T. *Nature* **1993**, *363*, 603−605.

(3) Bethune, D. S.; Kiang, C.-H.; de Vries, M. S.; Gorman, G.; Savoy, R.; Vazquez, J.; Beyers, R. *Nature* **1993**, *363*, 605−607.

(4) Huang, S.; Cai, X.; Liu, J. *J. Am. Chem. Soc.* **2003**, *125*, 5636−5637.

(5) Su, M.; Zheng, B.; Liu, J. *Chem. Phys. Lett*. **2000**, *322*, 321−326.

(6) Jeong, H. J.; An, K. H.; Lim, S. C., et al. *Chem. Phys. Lett*. **2003**, *380*, 263−268.

(7) Dai, H. *Acc. Chem. Res.* **2002**, *35*, 1035−1044.

(8) Dai, H. *Surf. Sci.* **2002**, *500*, 218−241.

(9) Thess, A., et.al.; Fischer, J.; Smalley, R. *Science* **1996**, *273*, 483−487.

(10) Tans, S. J.; Devoret, M. H.; Dai, H.; Thess, A.; Smally, R. E.; Geerligs, L. J.; Dekker, C. *Nature* **1997**, *386*, 474−477.

(11) Bladh, K.; Falk, L. K. L.; Rohmund, F. *Appl. Phys. A* **2000**, *70*, 317−322.

(12) Kong, J.; Soh, H.; Cassell, A.; Dai, H. *Nature* **1998**, *395*, 878−881.

(13) Hongo, H.; Nihey, F.; Ichibashi, T.; Ochiai, Y.; Yudasaka, M.; Iijima, S. *Chem. Phys. Lett.* **2003**, *380*, 158−164.

(14) Cassell, A. M.; Raymakers, J. A.; Kong, J.; Dai, H. *J. Phys. Chem. B* **1999**, *103*, 6484−6492.

(15) Puretzky, A. A.; Geohegan, D. B.; Fan, X.; Pennycook, S. J. *Appl. Phys. Lett.* **2000**, *76*, 182−184.

(16) Zhang, G. Y.; Ma, X. C.; Zhong, D. Y.; Wang, E. G. *J. App. Phys*. **2002**, *91*, 9324−9332.

(17) Gavillet, J.; Loiseau, A.; Journet, C.; Willaime, F.; Ducastelle, F.; Charlier, J. C. *Phys. Rev. Lett.* **2001**, *87*, 275504.

(18) Seidel, R.; Duesberg, G.; Unger, E.; Graham, A. P.; Liebau, M.; Kreupl, F. *J. Phys. Chem. B* **2004**, *108*, 1888−1893.

(19) Hornyak, G. L.; Grigorian, L.; Dillon, A. C.; Parilla, P. A.; Jones, K. M.; Heben, M. J. *J. Phys. Chem. B* **2002**, *106*, 2821−2825.

(20) Kwon, Y. K.; Lee, Y. H.; Kim, S.-G.; Jund, P.; Tománek, D.; Smalley, R. E. *Phys. Rev. Lett*. **1997**, *79*, 2065−2068.

(21) Nardelli, M. B.; Brabec, C.; Maiti, A.; Roland, C.; Bernholc, J. *Phys. Rev. Lett.* **1998**, *80*, 313−326.

(22) Lee, Y. H.; Kim, S. G.; Jund, P.; Tomanek, D. *Phys. Rev. Lett.* **1997**, *78*, 2393−2396.

(23) *Carbon Nanotubes: Synthesis, Structure, Properties and Application*; Dresselhaus, M. S., Dresselhaus, G., Avouris, Ph., Eds.; Springer: Berlin, 2001; pp 71−72.

(24) Shibuta, Y.; Maruyama, S. *Physica B* **2002**, *323*, 187−189.

(25) Alvarez, W. E.; Pompeo, F.; Herrera, J. E.; Balzano, L.; Resasco, D. E. *Chem. Mater*. **2002**, *14*, 1853−1858.

(26) Maruyama, S.; Kojima, R.; Miyauchi, Y.; Chiashi, S.; Kohno, M. *Chem. Phys. Lett*. **2002**, *360*, 229−234.

(27) Nikolaev, P.; Bronikowski, M. J.; Bradley, R. K.; Rohmund, F.; Colbert, D. T.; Smith, K. A.; Smalley, R. E. *Chem. Phys. Lett.* **1999**, *313*, 91−97.

(28) Puretzky, A. A.; Schittenhelm, H.; Fan, X.; Lance, M. J.; Allard, L. F., Jr.; Geohegan, D. B. *Phys. Rev. B* **2002**, *65*, 245425.

(29) Ostrovskii, O. I.; Grigoryan, V. A.; Visharev, A. F. *Svoystva metallitcheskih rasplavov*; Metallurgiya: MosKva, 1988; p 304.

(30) Walther, J. H.; Jaffe, R.; Halicioglu, T.; Koumoutsakos, P. *J. Phys. Chem. B* **2001**, *105*, 9980−9987.

(31) Brenner, D. W. *Phys. Rev. B* **1990**, *42*, 9458−9471.

(32) Beeler, J. R. *J. Adv. Mater. Res*. **1970**, *4*, 295−476.

(33) Evteev, A. V.; Kosilov, A. T.; Milenin, A. V. *Phys. Solidi Status* **2001**, *43*. 2284−2289.

(34) Yamamoto, R. Matsuoka, H.; Doyama, M. *J. Phys. Status Solidi* (*a*) **1978**, *45*, 305−314.

(35) Johnson, R. A. *Phys. Rev*. **1964**, *134*, A1329−36.

(36) Rosato, V.; Guillope, M.; Legrand, B. *Philos. Mag. A* **1989**, *59*, 321−336.

(37) Lewis, L. J.; Jensen, P.; Barrat, J−L. *Phys. Rev. B* **1997**, *56*, 2248−2257.

(38) Stanek, J.; Marest, G.; Ja.rezic, H.; Binczycka, H. *Phys. Rev. B* **1995**, *52*, 8414−8422.

(39) Guillope, M.; Legrand, B. *Surf. Sci.* **1989**, *215*, 577−595.

(40) Ding, F.; Bolton, K.; Rosén, A. *J. Vac. Sci. Technol. A* **2004**, *22*, 1471−1476.

(41) Durgun, E.; Dag, S.; Bagci, V. M. K.; Gulseren, O.; Yildirim, T.; Ciraci, S. *Phys. Rev. B* **2003**, *67*, 201401.

(42) Gutsev, G. L.; Bauschlicher, C. W., Jr. *Chem. Phys.* **2003**, *291*, 27−40.

(43)]. Scott, C. D.; Arepalli, S.; Nikolaev, P.; Smalley, R. E. *Appl. Phys. A* **2001**, *72*, 573−580.

(44) Berendsen, H. J. C.; Postma, J. P. M.; van Gunsteren, W. F.; DiNola, A.; Haak, J. R. *J. Chem. Phys*. **1984**, *81*, 3684−3690.

(45) Meyyappan, M.; Delzeit, L.; Cassell, A.; Hash, D. *Plasma Sources Sci. Technol*. **2003**, *12*, 205−216.

(46) Gavillet, J.; Loiseau, A.; Ducastelle, F.; Thair, S.; Bernier, P.; Stephan, O.; Thibault, J.; Charlier, J−C. *Carbon* **2002**, *40*, 1649−1663.

(47) Talanquer, V. *J. Chem. Educ.* **2002**, *79*, 877−883.

(48) Yuklyosi, K., Ed. *Encyclopedic Dictionary of Mathematics*; MIT Press: Cambridge, 1977.

(49) Kanzow, H.; Ding, A. *Phys. Rev. B* **1999**, *60*, 11180−11186.

(50) Kanzow, H.; Lenski, C.; Ding, A. *Phys. Rev. B* **2001**, *63*, 125402.

(51) Ci, L.; Xie, S.; Tang, D.; Yan, X.; Li, Y.; Liu, Z.; Zou, X.; Zhou, W.; Wang, G. *Chem. Phys. Lett.* **2001**, *349*, 191−195.

(52) Ago, H.; Oshima, S.; Uchida, K.; Yumura, M. *J. Phys. Chem. B* **2001**, *105*, 10453−10456.

(53) Moisala, A.; Nasibulin, A. G.; Kauppinen, E. I. *J. Phys: Condens. Matter* **2003**, *15*, 3011−3035.

(54) Mann, D. J.; Halls, M. D.; Hase, W. L. *J. Phys. Chem. B* **2002**, *106*, 12418−12425.